A Miniaturized Catheter 2-D Array for Real-Time, 3-D Intracardiac Echocardiography

Warren Lee, *Member, IEEE*, Salim F. Idriss, Patrick D. Wolf, *Member, IEEE*, and Stephen W. Smith, *Member, IEEE*

***Abstract*—The design, fabrication, and characterization of a 112 channel, 5 MHz, two-dimensional (2-D) array transducer constructed on a six layer flexible polyimide interconnect circuit is described. The transducer was mounted in a 7 Fr (2.33 mm outside diameter) catheter for use in real-time intracardiac volumetric imaging. Two transducers were constructed: one with a single silver epoxy matching layer and the other without a matching layer. The center frequency and −6 dB fractional bandwidth of the transducer with a matching layer were 4.9 MHz and 31%, respectively. The 50 Ω pitch-catch insertion loss was 80 dB, and the typical interelement crosstalk was −30 dB. The final element yield was greater than 97% for both transducers. The transducers were used to acquire real-time, 3-D images in an in vivo sheep model. We present in vivo images of cardiac anatomy obtained from within the coronary sinus, including the left and right atria, aorta, coronary arteries, and pulmonary veins. We also present images showing the manipulation of a separate electrophysiological catheter into the coronary sinus.**

I. Introduction

In intracardiac echocardiography (ICE), a catheter containing a miniature ultrasound transducer is directed into the heart, allowing the imaging of cardiac structures from an intracardiac viewpoint. The ICE imaging approach affords several advantages over more conventional transthoracic (TTE) and transesophageal (TEE) imaging as described in [1]. The close proximity of the transducer to the imaged structures circumvents the problems associated with TTE in patients with poor acoustic windows. In addition, ICE does not require general anesthesia and is more easily tolerated by patients than TEE. The utility of ICE has been chiefly in the area of visualizing cardiac structures and devices used during electrophysiological interventions. The applications of ICE in cardiac interventional procedures include: visualization of the left atrium and pulmonary veins during ablation treatment of atrial fibrillation [2], transcatheter closure of atrial septal defects [3]–[5]. For these treatments, ultrasound guidance has clear advantages over fluoroscopy as described in [6], including: the definition of cardiac anatomy, therapeutic device orientation with respect to anatomic locations, and verification of proper electrode-tissue contact. In addition, new procedures, such as biventricular pacing [7], [8], require lead implantation within or on the right and left ventricle [9]; where ICE may be useful in locating the coronary sinus, particularly in individuals with complicated cardiac anatomy.

There are currently two commercial catheter-based intracardiac probes used for clinical ultrasound B-scan imaging: a 9 Fr, 9 MHz rotating single-element catheter (Boston Scientific Corp., Fremont, CA) (1 Fr $\approx$ 0.33 mm) [2], and a 10 Fr, 5.5–10 MHz, phased-array ultrasound catheter (Acuson Corp., Mountain View, CA) [10]. A review of ICE using these devices can be found in [11]. Although these intracardiac transducers can be used to aid in the guidance of interventional cardiac procedures, both have limitations associated with the monoplanar nature of the B-scan images. Real-time 3-D (RT3D) imaging may overcome these limitations. In RT3D echocardiography, a 2-D array transducer is used to steer and focus the ultrasound beam over a pyramidal-shaped volume rather than a single-sector scan [12], [13]. Recent studies have demonstrated the effectiveness of RT3D echocardiography for the monitoring of left ventricular function [14], detection of perfusion defects [15], reduced scanning times in dobutamine stress echo exams [16], guidance of right ventricular endomyocardial biopsy [17], measurement of peak left ventricular flow velocities [18], and evaluation of congenital cardiac abnormalities [19].

In RT3D intracardiac imaging, the 2-D array transducer is miniaturized and mounted in a catheter, enabling the 3-D viewing of cardiac structures and interventional catheter devices in cross sectional and en face views [20]. Within the acquired volumes, multiple real-time B, C, or inclined planes can be displayed, as well as real time, 3-D-rendered images [21].

We previously described a 12 Fr, 64 channel side-viewing catheter 2-D array operating at 5 MHz [20], [22]–[24], a 9 Fr, 70 channel side-viewing catheter 2-D array operating at 7 MHz [25], and dual-lumen, forward-viewing 2-D array probes operating at 5 MHz [26]. In this paper, we describe advances toward smaller, more clinically useful catheter 2-D arrays with increased channel counts. The new transducer was mounted in a 7 Fr catheter and contains 112 channels operating at 5 MHz. Advanced registration technology allowed the interconnect to be constructed on multiple, miniaturized, laminated, flexible polyimide layers. We also have incorporated a high-density, noncoaxial, ribbon-based cabling interconnection in the catheter

Manuscript received July 10, 2003; accepted June 16, 2004. This research was supported by the NIH (grants HL64962 and HL58754) and NSF (grant DMR0104304).

W. Lee, P. D. Wolf, and S. W. Smith are with the Department of Biomedical Engineering, Duke University, Durham, NC. W. Lee currently is with the General Electric Company, Niskayuna, NY 12309 (e-mail: lee@research.ge.com).

S. F. Idriss is with the Department of Pediatrics, Duke University Medical Center, Durham, NC.

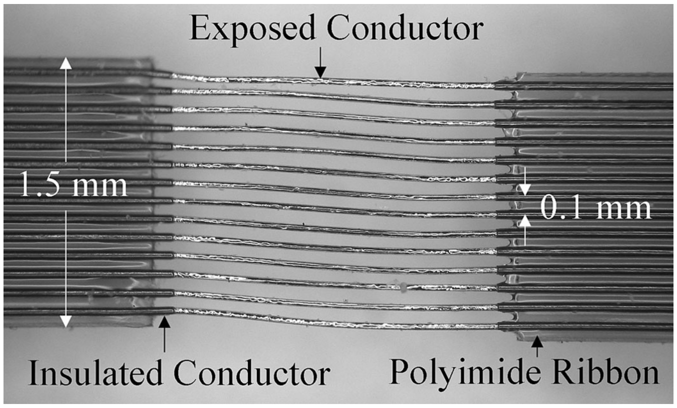

Fig. 1. Photograph of a single MF ribbon cable showing relevant dimensions.

lumen. By using the advanced, multisignal layer, high-density, flexible transducer interconnect, and the high-density, ribbon-based, catheter-cabling interconnect, we have been able to implement a higher channel count and a smaller, more clinically useful catheter size for RT3D intracardiac imaging. In addition, the small size of the imaging catheter allowed RT3D imaging from within the coronary sinus for the first time, a stable location from which the left atrium and pulmonary veins may be viewed.

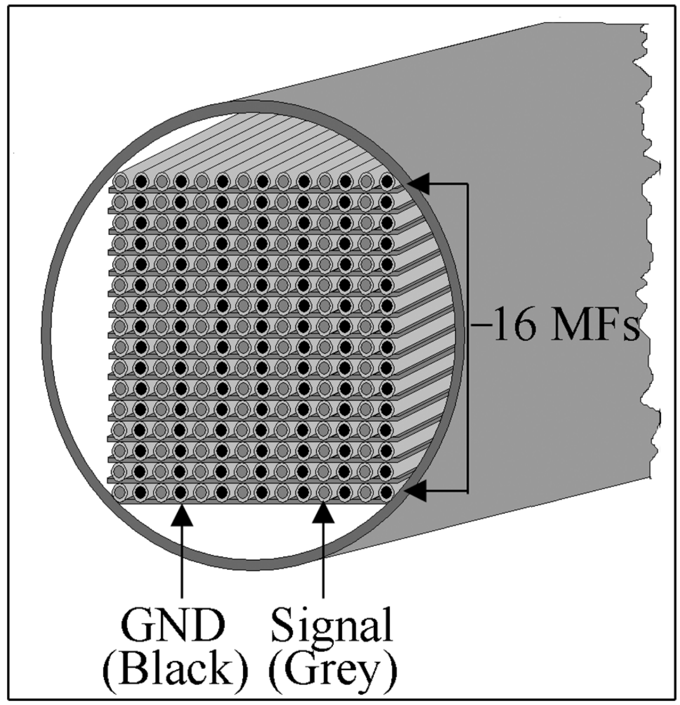

Fig. 2. Schematic catheter cross section. The catheter contains 16 Microflat^{TM} ribbons (MF), each with 14 conductors in an alternating signal (grey) and GND (black) pattern.

II. Methods

A. Design and Simulation

Driven by the motivation toward a smaller catheter size, our primary design constraint was the number of cables that would fit inside the 1.98-mm inner diameter of the 7 Fr catheter. In order to maximize the number of active elements in our transducer design under such severe size constraints, we chose to use a high-density, MicroFlat^{TM} (MF) cabling interconnection (W. L. Gore & Associates, Pleinfeld, Germany). The ribbon-based MF cables contain 14 insulated conductors on 0.1-mm spacing bound to a polyimide substrate. When the MF ribbons are stacked, the vertical spacing between conductors is also 0.1 mm. The individual conductors are approximately 40 μ in diameter, and are individually insulated. A photograph of a single MF ribbon is shown in Fig. 1.

It was determined that the 1.98 mm inner diameter of the 7 Fr catheter would accommodate 16 MF ribbons. To reduce the interelement crosstalk, the MF cabling was used in an alternating, signal-ground configuration, which implied that there were seven conductors on each MF cable available for connection to a signal pad. Thus, there were a maximum of $16 \times 7 = 112$ active channels in our array design. Fig. 2 is a schematic of the catheter cross section, showing the 16 MF ribbons each containing 14 conductors in an alternating signal (grey circles) and ground (black circles) pattern.

Although the maximum number of active elements in the transducer design was determined by the packing density of the cables, the overall aperture size of the transducer was determined by space constraints in the 7 Fr catheter. Due to the low sensitivity of the small 2-D array elements, only those array patterns that incorporated the maximum number of 112 active elements in both transmit and receive were considered. System bandwidth restricted the maximum operating frequency of the transducer to 5 MHz. Table I summarizes the parameters associated with the 2-D array elements. The interelement pitch was equivalent to a $\lambda/2$ dense sampling, assuming a sound speed of 1500 m/s. The lead zirconate titanate (PZT) thickness necessary for a 5 MHz resonant frequency was determined to be 0.290 mm. Assuming the saw kerf was 0.03 mm wide, the resulting element width-to-thickness ratio was sufficient to decouple the width and length mode resonances from the desired thickness mode resonance.

TABLE I
2-D Element Parameters.

Quantity	Symbol	Value
Operating frequency	f_0	5.0 MHz
Interelement spacing	d	0.15 mm
Element thickness	t	0.29 mm
Element width	w	0.12 mm
Width/thickness ratio	w/t	0.41
Element length	l	0.12 mm
Length/thickness ratio	l/t	0.41

The coordinate system used in the volumetric scanner was described in [12]. The pyramidal volume can be

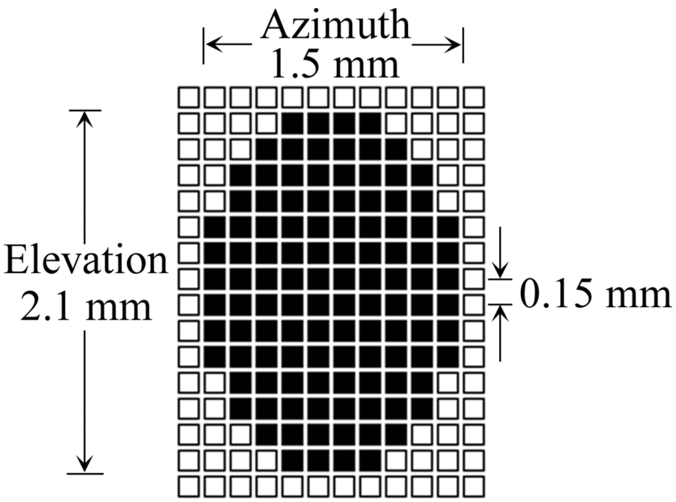

Fig. 3. The 2-D array geometry with 112 channels on 0.15-mm spacing. The active elements are shown as filled squares. The aperture size in azimuth and elevation is 1.5 mm and 2.1 mm, respectively.

scanned from either the azimuth or elevation. For reference purposes, in this paper the azimuth and elevation directions were defined as the directions perpendicular and parallel to the catheter long axis, respectively. To simulate beam shapes resulting from candidate array geometries, Field II software developed by Jensen and Svendsen [27] was used. The simulations assumed a Gaussian-shaped excitation centered at 5 MHz with a 30% −6 dB fractional bandwidth. Our fabrication processes require at least one row of inactive elements surrounding the active elements on all sides of the array. Therefore, the maximum aperture size in azimuth that was available for active elements was the 7 Fr catheter inner diameter minus twice the interelement spacing, or 1.98 mm − 2 × 0.15 = 1.68 mm. Fig. 3 shows the array pattern, selected based on main lobe width, sensitivity, and low off-axis clutter. The transducer has an aperture size of 1.5 mm in azimuth and 2.1 mm in elevation. The Field II simulated on-axis azimuth and elevation beamplots resulting from the selected array pattern are shown in Fig. 4.

Figs. 4(A) and (B) indicate that the −6 dB beamwidths in the azimuth and elevation dimensions are approximately 12°, and 9°, respectively. The narrower beamwidth in elevation was due to its slightly larger aperture. For angles greater than ±30°, a −55 dB clutter floor exists. Figs. 4(C) and (D) show the −6 dB and −20 dB azimuth and elevation beamwidths in millimeters versus depth. The small aperture of the catheter transducer results in a far-field transition distance of $D^2/4\lambda = (1.5\text{ mm})^2/4(0.3\text{ mm}) \approx$ 2 mm in azimuth and $(2.1\text{ mm})^2/4(0.3\text{ mm}) \approx 4$ mm in elevation. Thus, the radiation pattern of the transducer is essentially that of a planar piston in the far-field. However, at short ranges, the simulations indicate that the beamwidth still should be sufficiently small to resolve important cardiac structures. We note that, at a depth of 1 cm, the −6 dB and −20 dB beamwidths are 2.1 mm and 3.8 mm for the azimuth direction, and 1.5 mm and 2.6 mm for the elevation direction.

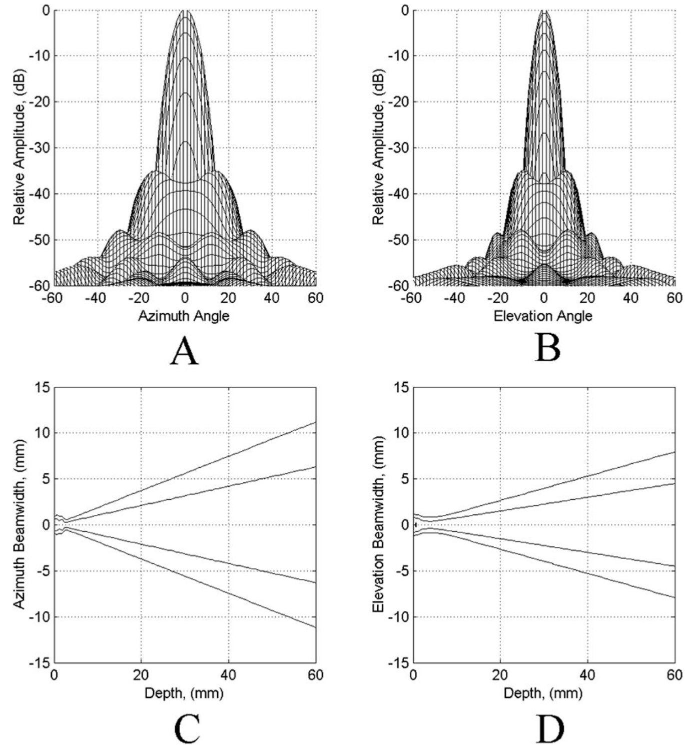

Fig. 4. Simulated pulse-echo azimuth and elevation beamplots. (A) and (B) Azimuth and elevation beamplots versus angle. (C) and (D) −6 dB and −20 dB azimuth and elevation beam contours versus depth in millimeters.

In order to simulate the thickness mode resonant behavior of the 2-D array element, we used the Krimholtz, Leedom, and Matthaei (KLM) model [28]. Two simulations were performed: one for the transducer without a matching layer (7FnoML), and the other for the transducer with a 60-μm thick Ag epoxy matching layer (7FML). The modeled layers and their thicknesses are shown in Fig. 5. The flex circuit was modeled as a single polyimide layer of equivalent total thickness, as the internal conductor ($< \lambda/20$ thickness) and bond layers were found not to have a significant effect on the results. Two flex circuits were included in the transducer backing due to the fact that the distal end of the flex circuit was bent around the proximal end during final assembly. The simulations included a 3 pF shunt capacitance representing the trace capacitance of the flex circuit, and a 1-m long cable (76 Ω, 1000 dB/km attenuation at 10 MHz) representing the MF cabling. A 50 Ω transmitter output impedance, and 100 Ω receiver input impedance were included in the simulations. Table II lists the modeled layers and relevant material properties and their thicknesses for the two cases, with the top layer listed first and the bottom layer listed last. The PiezoCAD (Sonic Concepts, Woodinville, WA) listed bar mode velocity was used for the PZT5H layer, and the velocity for the Ag epoxy matching layer was obtained by fitting to experimental data with a known geometry and density.

Fig. 7 shows the results of the simulation, with the pulse-echo impulse response and power spectrum for 7FnoML in Fig. 7(A) and (B), and for 7FML in Fig. 7(C)

TABLE II
THE KLM SIMULATION PARAMETERS FOR THE 7FML AND 7FNOML TRANSDUCERS.

Layer	Long velocity (m/s)	Density (kg/m^3)	Loss (dB/cm)	Thickness (μm)	Layer in 7FML?	Layer in 7FnoML?
Liquid crystal polymer (LCP)	1340	1400	N/A[1]	11	Yes	No
Epoxy bond	2600	1100	N/A	2	Yes	No
Ag epoxy ML	1100	2650	N/A	60	Yes	No
Silver foil	3600	10500	N/A	7	No	Yes
Ag epoxy bond	1900	2650	N/A	5	No	Yes
PZT5H (bar mode)	3850	7500	elect. loss 0.02 mech. loss 0.015	290	Yes	Yes
Ag epoxy bond	1900	2650	N/A	5	Yes	Yes
Copper	4660	8930	N/A	5	Yes	Yes
Polyimide flex	2200	1410	N/A	200	Yes	Yes
D236 Acoustic backing	1400	1500	140	500	Yes	No
Filled epoxy	2450	1100	54	500	No	Yes
Polyimide flex	2200	1410	N/A	200	Yes	Yes
Nylon catheter	2770	1140	3.2	175	Yes	Yes

[1]Not applicable.

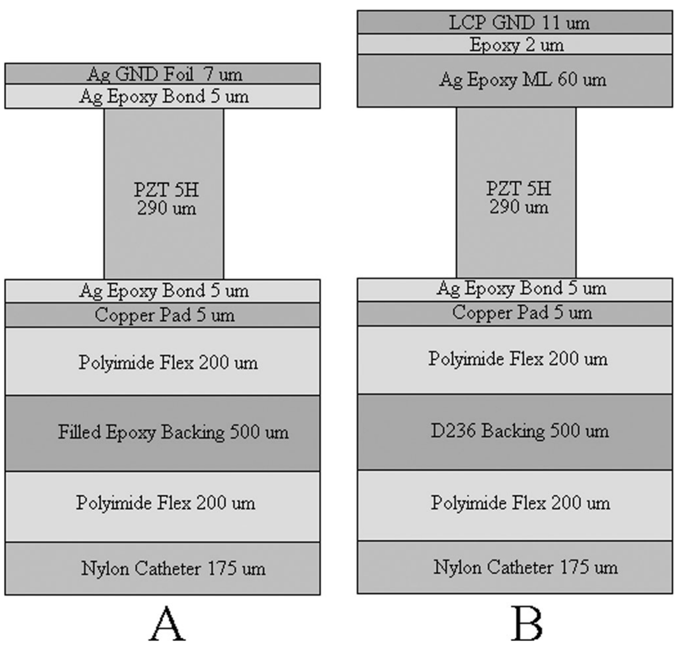

Fig. 5. The KLM modeled layers and thicknesses: (A) without matching layer, (B) with 60 μm thick Ag epoxy matching layer.

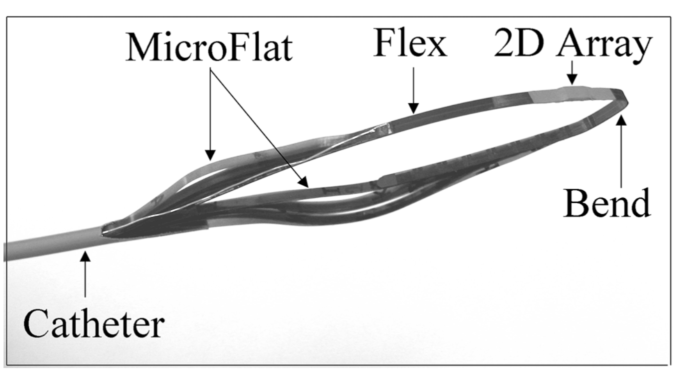

Fig. 6. The MF cable assembly terminated to flex interconnect, showing bend of flex interconnect.

and (D). The simulated center frequency and −6 dB fractional bandwidth of the 7FnoML and 7FML transducers are 4.3 MHz, 25%, and 4.5 MHz, 34%, respectively. The simulations indicate that the addition of the matching layer should increase the transducer sensitivity by 6 dB. The ringing in the vicinity of 1.5–2 μs in Fig. 7(C) was due to the incomplete attenuation of the echoes propagating into the transducer backing. This was verified by increasing the simulated backing thickness, which eliminated the ringing.

B. Interconnect Fabrication

In order to accommodate the dense sampling of the transducer elements under the size constraints of the 7 Fr catheter, a six-layer, flexible, interconnect circuit was fabricated by MicroConnex (Snoqualmie, WA). Fig. 8 shows a schematic cross section of the flex circuit.

The flex circuit consists of three layers of polyimide bonded together with two layers of acrylic bondply. Metal layers 2–5 were first fabricated using subtractive photolithography methods on three presputtered and electroplated polyimide substrates. The polyimide layers then were laminated together using the acrylic bondply. Following the polyimide lamination, 50 μ diameter vias were formed by laser drilling with subsequent metallization. Metal layers 1 and 6 then were patterned using subtractive photolithography; and a 25 μ thick covercoat (not shown) was applied over the bottom layer. Details of the flex circuit fabrication can be found in [29].

Electrical connections to the 2-D array elements and solder connections to the cabling assembly were made on the topmost metal pad layer. Metal layers 2–6 are signal layers, in which 25 μ wide traces were routed from array elements to solder pads (not shown). Fig. 9 shows a photograph of the completed flex circuit, including a close-up of the solder pads and a close-up of the array pads. A ground bus accompanies each row of signal solder pads. The sol-

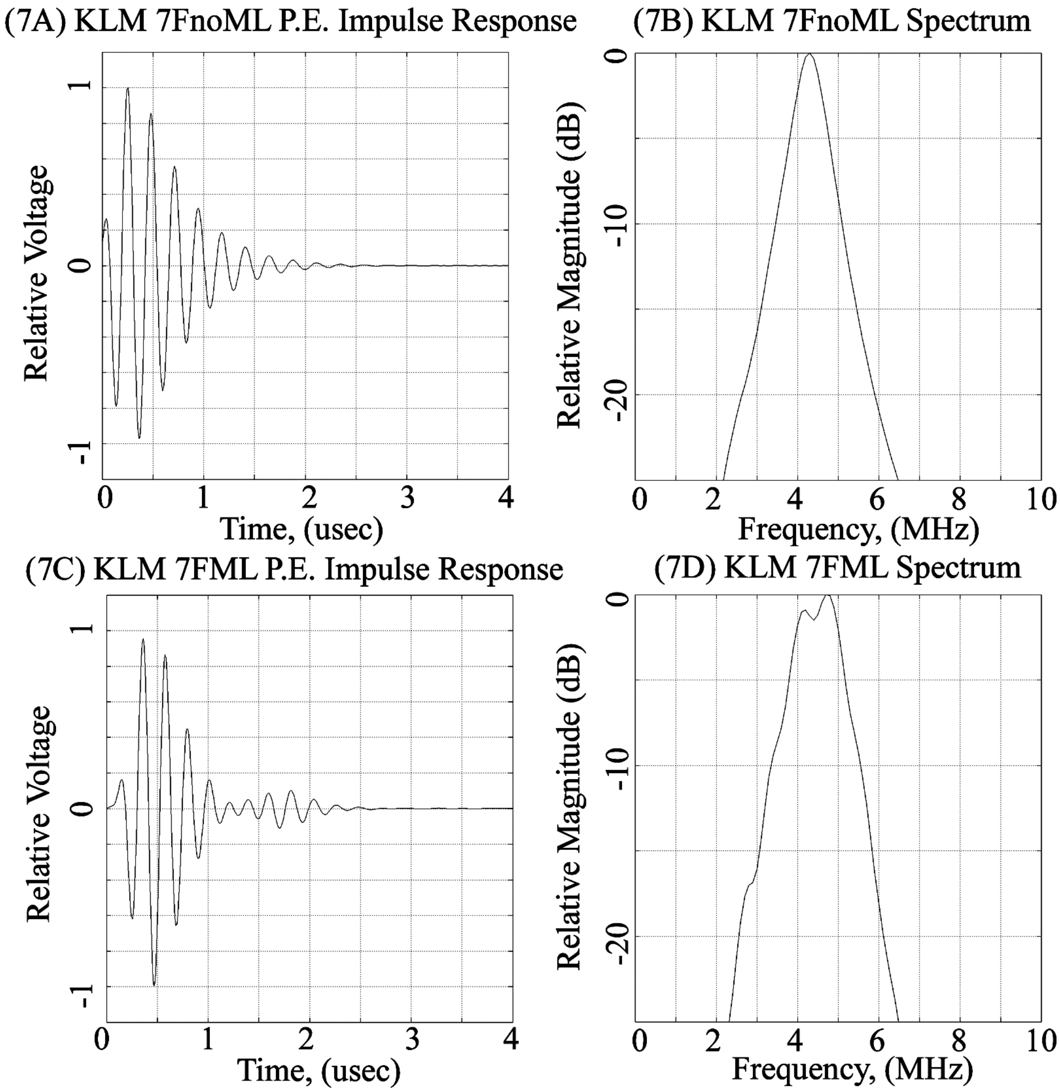

Fig. 7. The KLM simulation results. (A) and (B) impulse response and spectrum for the 7FnoML transducer; (C) and (D) for the 7FML transducer. The simulated center frequency and −6 dB fractional bandwidth is 4.3 MHz, 25% for the 7FnoML transducer, and 4.5 MHz, 34% for the 7FML transducer.

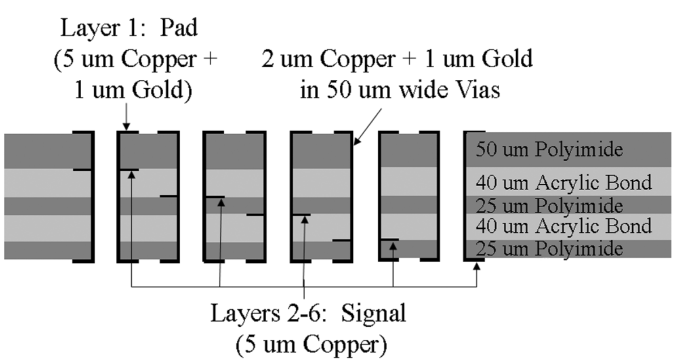

Fig. 8. Longitudinal cross section of flex circuit.

der pads have a spacing of 250 μ, and the array elements have a spacing of 0.15 mm. The flex circuit is 1.9-mm wide, 80-mm long, and 0.2-mm thick.

C. Transducer Fabrication

Two transducers were fabricated: one with a single matching layer (7FML) and the other without a matching layer (7FnoML). A conductive silver epoxy served as the matching layer for the 7FML transducer. The silver epoxy matching layer was cast onto a plate of PZT5-H (TRS Ceramics, State College, PA), vacuum degassed, and allowed to cure at a slightly elevated temperature, resulting in an initial matching layer thickness of 150 μm. A 2.6-mm by 2.3-mm piece of the PZT with matching layer then was cut from the plate, and the matching layer then was ground down using a surface grinder (Model MSG-200MH, Mitsui High-Tec Inc., Kitakyushu, Japan) and hand lapped to a final thickness of 60 μm. During hand lapping, the matching layer thickness was monitored using a thickness gauge (Model MT 60 M, Heidenhain, Schaumburg, IL). The variation of the final matching layer thickness over the 2.6-mm by 2.3-mm area was measured to be less than 5%.

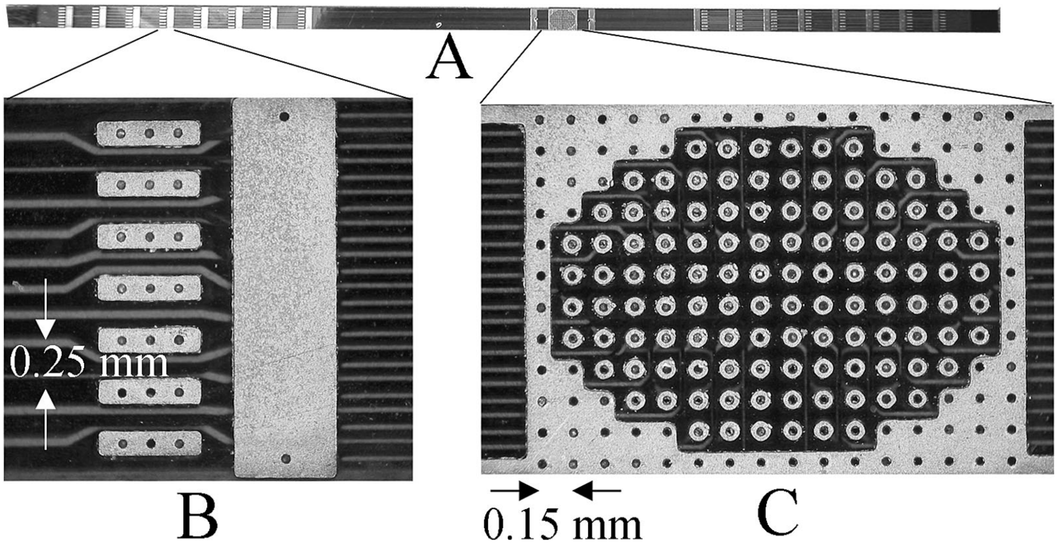

Fig. 9. (A) Photograph of completed flex circuit. (B) Close-up of solder pads spaced 0.25 mm apart, (C) close-up of array pads spaced 0.15 mm apart.

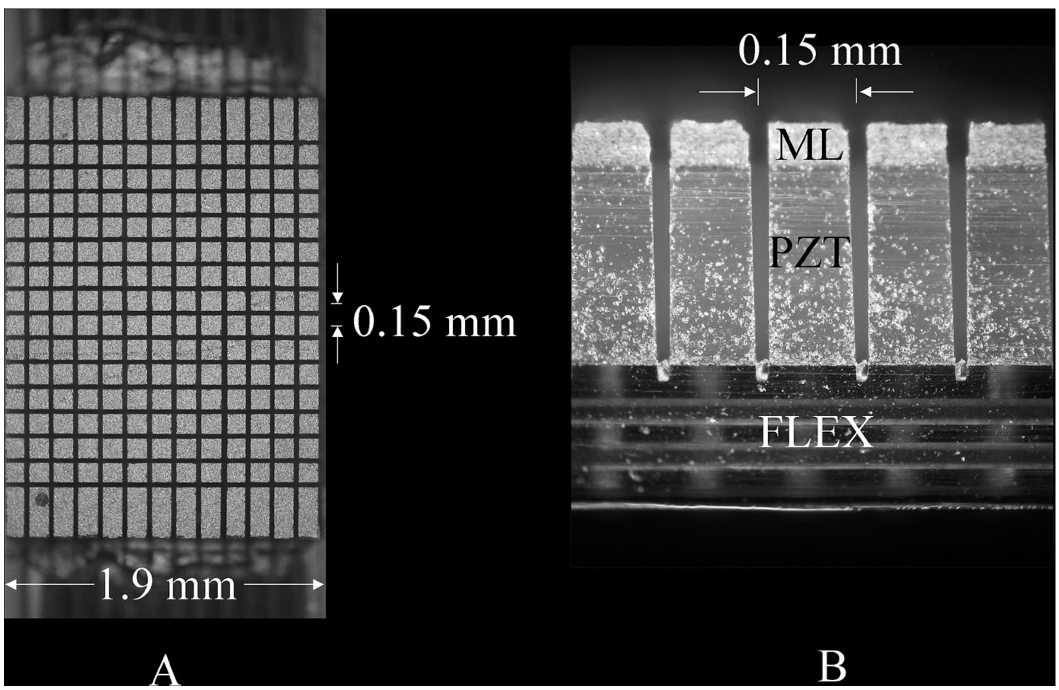

Fig. 10. (A) Top view of the 7FnoML diced array. (B) Side view of the diced 7FML array.

Fabrication of the 7FnoML and 7FML transducers on the flexible interconnect circuit then proceeded as described in [23] and [30] and summarized here. The PZT was bonded to the interconnect using conductive silver epoxy (Part # 50-10-0584-0029, Chomerics, Woburn, MA). The individual elements were formed by dicing with a diamond dicing saw (Model 780, Kulicke and Soffa, Willow Grove, PA). The saw kerf extended into, but not through, the 50-μm thick top polyimide layer. Fig. 10(A) shows a top view of the 7FnoML diced array on the flex circuit. A side view of the 7FML diced array is shown in Fig. 10(B). In Fig. 10(B), various layers in the transducer can be seen, including the matching layer, PZT, flex circuit, and the saw kerf extending into the top sacrificial polyimide layer.

Common ground electrodes were bonded to the surface of the elements following dicing of the transducers. The 7FnoML transducer used our previous fabrication techniques in which a 7-μm thick silver foil layer was bonded to the elements with a conductive silver epoxy. The 7FML transducer used an 11-μm thick liquid crystal polymer (LCP) film containing a 0.25-μm thick layer of sputtered gold on one side as the common ground electrode. The LCP was bonded to the elements using a thin layer of nonconductive epoxy. The LCP, with its low acoustic impedance (Z_{LCP} = 1.8 Mrayl) was shown by KLM simulations to yield improved bandwidth and sensitivity when compared to the silver foil (Z_{silver} = 38 Mrayl). In addition, the lack of pinhole defects made the LCP desirable for physical isolation from the intracardiac environment. Following bonding of the ground (GND) layer, the edges of the ground electrodes in both cases were trimmed and sealed to the flex interconnect with nonconductive epoxy.

Completion of the fabrication of both the 7FML and 7FnoML transducers then proceeded as follows. A small window was cut from the side of the 7 Fr catheter lumen (Guidant Corporation, Indianapolis, IN) where the transducer array eventually would be located. A total of 16 MF ribbons were fed through the 1-m long catheter. Eight MF ribbons were terminated to the solder pads on one side of the flex circuit by hand soldering. The flex circuit then was bent backward around itself as shown in Fig. 6, and the remaining eight MF ribbons were terminated to the solder pads on the far end of the flex circuit.

After cable termination was completed, the transducer and cabling assembly were partially retracted into the lumen of the 7 Fr catheter. The 7FnoML transducer used a tungsten-filled epoxy backing that was injected into the transducer backing. The 7FML transducer used a low viscosity silicone-based acoustic backing (236 Dispersion Coating, Dow Corning, Midland, MI) as reported in [31]. The KLM simulations indicate that the filled epoxy backing resulted in slightly improved bandwidth; however, the 236 Dispersion Coating was desirable due to its lower viscosity and concomitant ability to fill small gaps in the transducer backing. The transducer and cabling assembly then were retracted fully into the lumen of the 7 Fr catheter. Additional acoustic backing was used to fill and seal the gaps between the flex circuit and the catheter lumen.

The proximal end of the MFs were terminated onto a double-sided connector, which in turn led through the system cable assembly onto an ITT Cannon Model DLM6-360P (White Plains, NY) connector, and into the 3-D scanner. The distal end of the completed 7FML catheter is shown in Fig. 11.

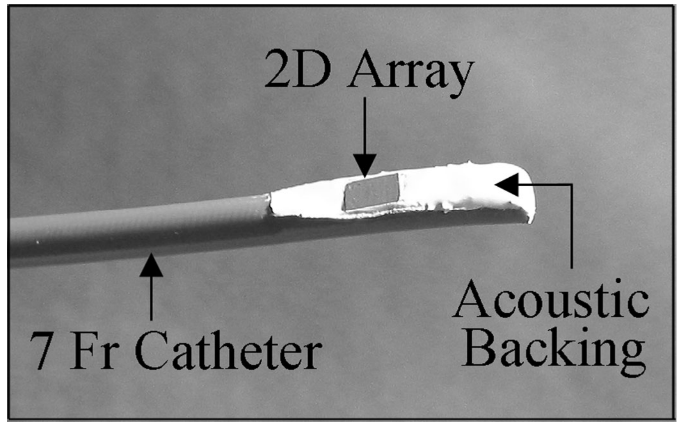

Fig. 11. Completed 7FML, 112 channel, 5 MHz 2-D catheter array.

D. Measurements

The impulse response and power spectrum, 50 Ω insertion loss, and interelement crosstalk were measured in order to characterize the 7FML and 7FnoML transducers. The impulse response was obtained by transmitting with a Panametrics Model 5073PR pulser/receiver (Waltham, MA), and observing the reflection from an aluminum block with a 10 pf Tektronix probe (Wilsonville, OR) into a Tektronix Model TDS744A Digitizing Oscilloscope. The spectrum was obtained by using a Panametrics 5605A Stepless Gate and a Hewlett-Packard Model 3588A Spectrum Analyzer (Palo Alto, CA).

The 50 Ω pitch-catch insertion loss at the end of the ITT Cannon connector (ITT Industries, White Plains, NY) was measured using a Hewlett-Packard Model 8165A Programmable Signal Source Generator (Hewlett-Packard, Palo Alto, CA) and an ENI model 325LA RF Power Amplifier (Rochester, NY) with a 50 Ω output impedance to generate a 10-cycle burst at 5 MHz on a transmit element. An aluminum block at a range of 5 mm was used to reflect the transmitted signal into a receive element loaded by a scope probe with an input impedance of 50 Ω.

Interelement crosstalk measurements at the end of the ITT Cannon connector were made by transmitting on a single element and measuring the crosstalk on other elements. The elements were loaded with the catheter cable assembly and the system cable, and terminated with 60 pF in parallel with 20 kΩ to simulate system loading. The crosstalk was measured on several different elements, including those adjacent to the transmitting channel on the transducer array, elements adjacent on the ITT Cannon system connector, and elements with adjacent conductors in the catheter cable bundle.

E. Animal Model

The in vivo images in this study were acquired using a sheep model. The study was approved by the Institutional Animal Care and Use Committee at Duke University and conformed to the Research Animal Use Guidelines of the American Heart Association. Ketamine hydrochloride (15–22 mg/kg of intramuscularly injected) was used to sedate the animals. A 20-gauge, intravenous catheter was placed in the saphenous vein for the purpose of intravenous fluid administration, and the animal was placed on a water heated thermal pad. The animals were anesthetized and mechanically ventilated with a mixture of 95–99% oxygen and 1–5% isoflurane. A nasogastric tube was passed to evacuate the stomach. A femoral arterial line was placed via a percutaneous puncture, and electrolyte and respirator adjustments were made based on serial electrolyte and arterial blood gas measurements. Sodium chloride 0.9% was intravenously infused continuously as a maintenance fluid. Throughout the procedure, the electrocardiogram, blood pressure, and temperature were continuously mon-

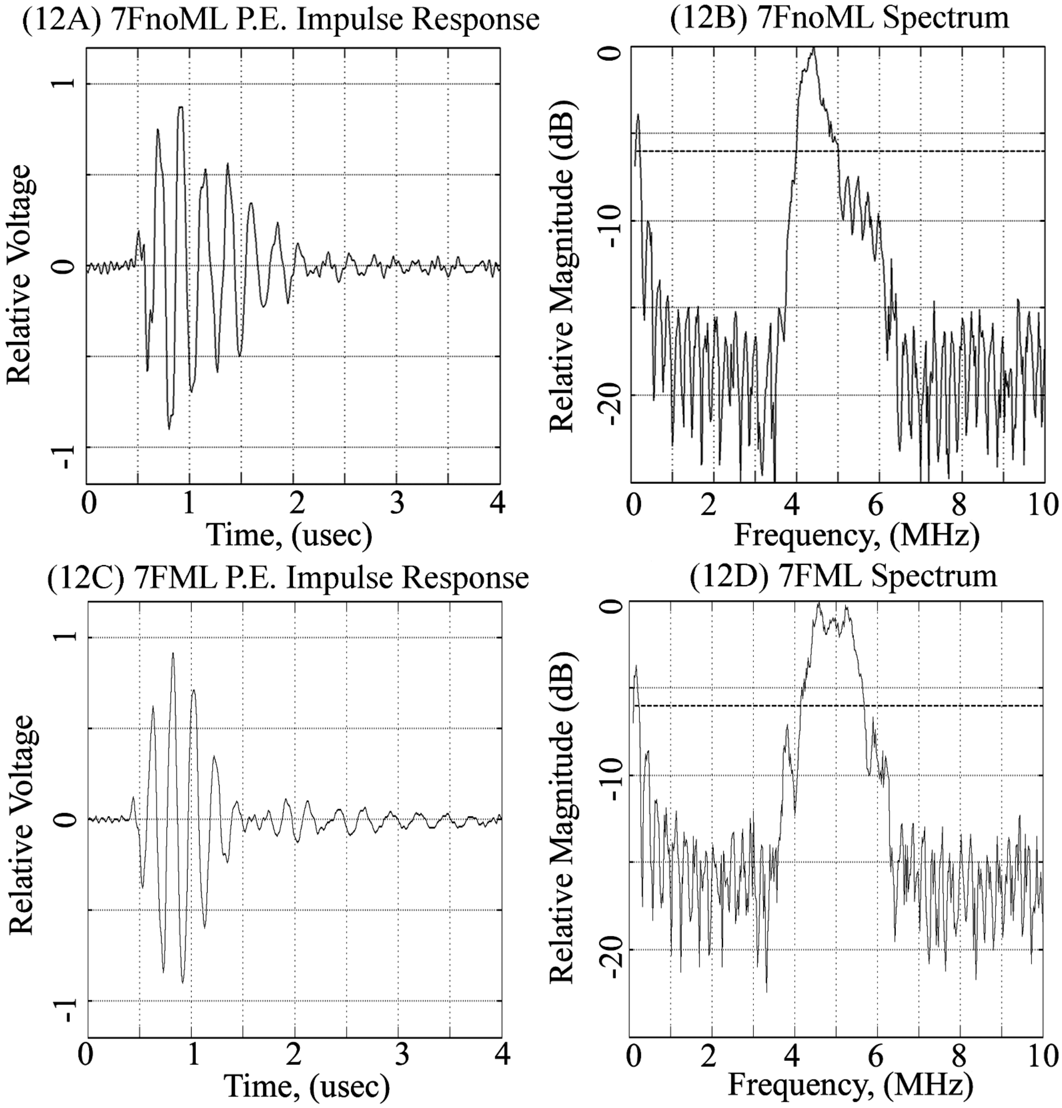

Fig. 12. Illustrative experimental impulse response and spectrum. (A) and (B) impulse response and spectrum for the 7FnoML transducer; (C) and (D) for the 7FML transducer. The center frequency and −6 dB fractional bandwidth is 4.5 MHz, 22% for the 7FnoML transducer, and 4.9 MHz, 31% for the 7FML transducer.

itored. For the open chest procedures, the heart was exposed by median sternotomy.

F. Intracardiac Echocardiography

Both closed and open chest sheep models were used in the course of obtaining our images. Closed chest experiments demonstrated the capability of using the 7 Fr imaging catheter in a clinical setting. The open chest model allowed manual palpation to be used to confirm the relative location and orientations of the transducer probe with respect to the cardiac structures imaged. The images shown include user selected B-scans, C-scans, and rendered volumes. In figures in which C-scans are shown, the C-scan plane is defined by arrows to either side of the B-scans. In figures in which rendered images are shown, the rendered volume is defined by the data in between the arrows that are at the side (or below) of the B-scans. White dots on the right side of the B-scans indicate 1-cm depth increments. It should be noted that the scales for the B-scans do not correspond to the rendered images, and the rendered images should not, in general, be used for measurements.

III. Results

A. Transducer Characterization Results

Table III lists the results of the characterization tests for the 7FML and 7FnoML transducers. The results from 10 elements were averaged in the reported data.

The crosstalk performance of the transducer assembly was similar in magnitude to our previous reports using micro-coaxial cabling [23] and virtual coaxial cabling [25]. A crosstalk level of −30 dB was observed for elements adjacent on the flex circuit, horizontally adjacent in the

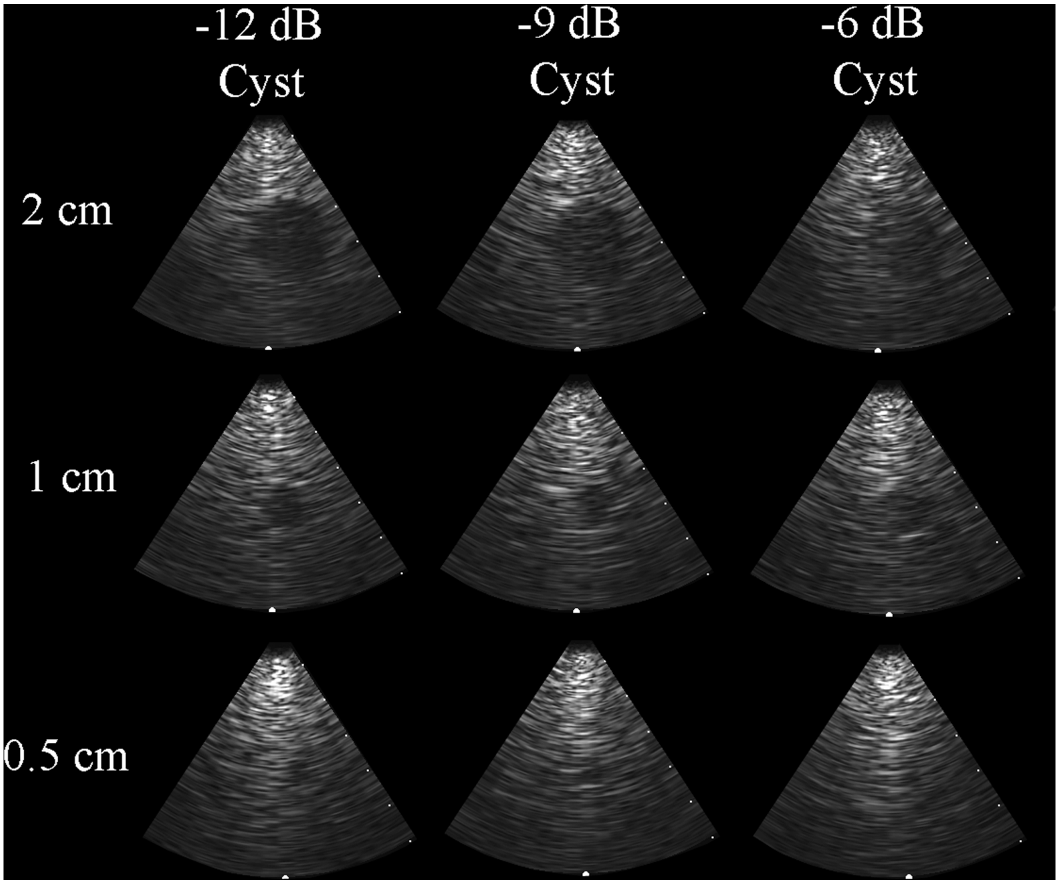

Fig. 13. Contrast detail study hypoechoic target images; 60°, 6-cm deep elevation scans are shown. Nine hypoechoic targets were imaged, ranging in echogenicity from −12 dB to −6 dB, and in diameters ranging from 2 cm to 0.5 cm.

TABLE III
Results of Experimental Transducer Characterization Tests.

Transducer	Center frequency	−6 dB fractional bandwidth	50 Ω insertion loss
7FML	4.9 MHz	31% ± 4%	−80 dB
7FnoML	4.5 MHz	22% ± 4%	−83 dB

MF cable bundle, and adjacent on the ITT Cannon connector. For those elements not adjacent on the flex, horizontally adjacent in the MF bundle, and adjacent on the ITT Cannon connector, the crosstalk level was less than −30 dB, and depended on the separation. Oakley *et al.* [32] also reported similar, albeit lower, levels of crosstalk when comparing miniature ultrasound probes constructed using both coaxial and MF cabling. For the 7FML and 7FnoML transducers, the worst case of −25 dB crosstalk occurred for two signal conductors vertically adjacent in the cable bundle, possibly due to the lack of a ground conductor in between the signal conductors. By staggering the vertical arrangement of the MF cables so that each signal conductor is surrounded on all four sides by a ground conductor, the crosstalk level may be reduced. The experimental insertion loss of the 7FML transducer was 80 dB compared to the 83 dB insertion loss for the 7FnoML transducer. The KLM model predicted a slightly higher 6 dB improvement in sensitivity.

Fig. 12 shows an illustrative experimental pulse-echo impulse response and spectrum from the 7FnoML and 7FML transducers. The center frequencies and −6 dB fractional bandwidths for the 7FnoML and 7FML transducers were 4.5 MHz, 22%, and 4.9 MHz, 31%, respectively. The experimental impulse response and spectrum of each transducer was reasonably close to the KLM simulations that predicted a −6 dB fractional bandwidth for the 7FnoML and 7FML transducers of 4.3 MHz, 25%, and 4.5 MHz, 34%. The discrepancies of the simulated and experimental data may have been due to the approximations of modeling the multilayer flex circuit as a single polyimide layer, and of using the 1-D model for a 2-D array element. The ringing in the vicinity of 2–3 μs in the 7FML impulse response was most likely due to the reverberation of echoes in the transducer backing, as indicated in the KLM simulations. Due to the severe space limitations inside the 7 Fr catheter lumen, only a small amount of acoustic backing could be injected into the transducer backing, and its actual thickness could only be approximated.

B. Images

By interfacing the 7 Fr, 2-D array imaging catheters with a 3-D scanner (Model 1, Volumetrics Medical Imag-

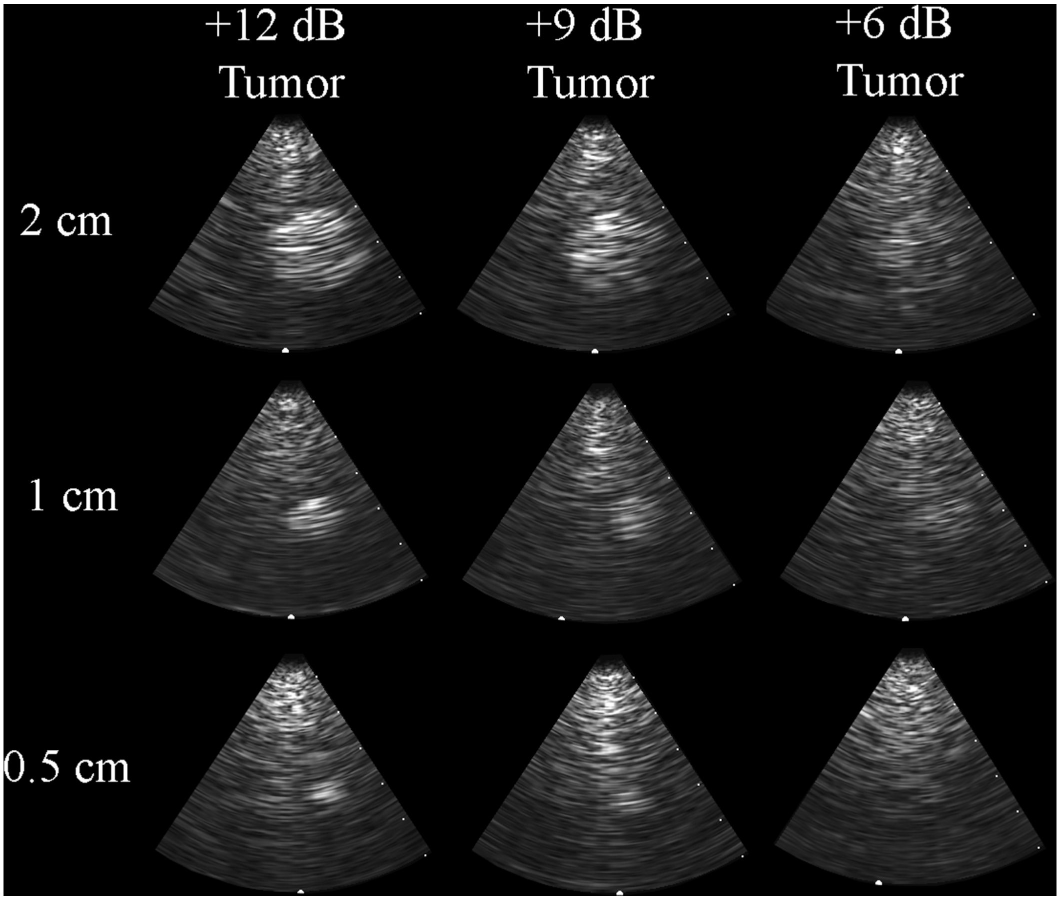

Fig. 14. Contrast detail study hyperechoic target images. Nine hyperechoic targets were imaged, ranging in echogenicity from +12 dB to +6 dB, and in diameters ranging from 2 cm to 0.5 cm.

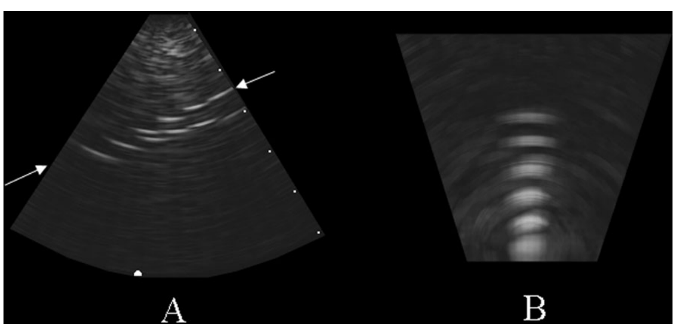

Fig. 15. CIRS wire phantom images: (A) 60°, 6-cm B-scan showing "<" shape of CIRS wire phantom. (B) Simultaneous, tilted C-scan taken at the arrows indicated in B-scan showing six wires.

ing, Durham, NC), we obtained real-time, 3-D scans of tissue mimicking phantoms and in vivo images of sheep heart. Twelve bit dynamic range was available at the detector input.

Figs. 13 and 14 show the results of a contrast detail study [33] using a cylindrical contrast resolution phantom (ATS Labs, Bridgeport, CT) in which the 7FML catheter transducer was used to image hypo- and hyperechoic targets of varying echogenicity and size. The transducer was oriented such that the hypoechoic and hyperechoic targets were imaged in 60°, 6-cm deep elevation scans. The hypoechoic regions ranged in echogenicity from −12 dB to −6 dB, and the hyperechoic regions ranged in echogenicity from +12 dB to +6 dB. The diameters of the hypo- and hyperechoic cross sections ranged from 2 cm to 0.5 cm. The results indicate that the spatial and contrast resolution of the transducer should be sufficient, particularly at short ranges, to detect important cardiac structures such as the coronary sinus and pulmonary veins.

Fig. 15(A) shows a 60°, 6 cm deep elevation B-scan of the CIRS tissue-mimicking phantom (CIRS Inc., Norfolk, VA). The phantom contains two sets of six wires arranged in a "<" shape. The axial spacing of the wires from right to left in the image is 5, 4, 3, 2, 1, and 0.5 mm. From the image, we see that the 7FML transducer has axially resolved the 2-mm targets. The lateral resolution at a depth of 3 cm was approximately 5 mm, in agreement with the simulated −6 dB beamwidth shown in Fig. 4(D). Fig. 15(B) is a simultaneous tilted C-scan taken at the level indicated in the B-scan showing six wires spaced 5 mm apart.

The images in Figs. 16 and 17 were obtained during in vivo sheep studies. In Fig. 16, the 7FnoML imaging catheter was guided into the right atrium and observed the insertion of a separate electrophysiological catheter (EP) into the coronary sinus (CS), a procedure analogous to CS lead placement in biventricular pacing. Figs. 16(A) and (B) are simultaneous, orthogonal 60°, 6-cm B-scans show-

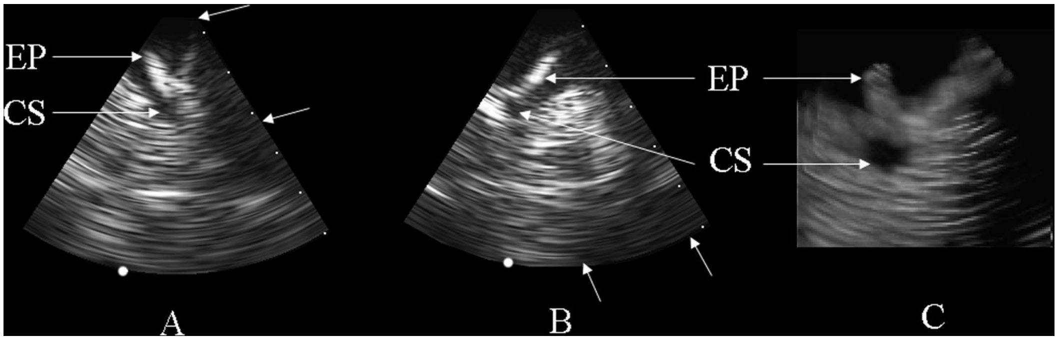

Fig. 16. In vivo sheep heart images: manipulation of an electrophysiological catheter (EP) into the coronary sinus (CS). (A), (B) 60°, 6-cm simultaneous, orthogonal B-scans showing EP catheter inserted into CS. (C) Simultaneous real-time 3-D rendered view taken in between the level of the arrows indicated in (A) and (B) showing EP catheter manipulation into the CS opening.

ing the EP catheter being inserted into the CS. Fig. 16(C) is a simultaneous 3-D rendered volume taken between the arrows indicated in Fig. 16(A) and (B) in which the insertion of the EP catheter into the CS opening can be seen. The ability of the intracardiac imaging catheter to visualize the EP catheter and CS opening in the 3-D rendering view greatly eased the guidance of the EP catheter into the CS.

The small size of the 7 Fr imaging catheters enabled RT3D intracardiac imaging from within the coronary sinus, a standpoint not possible with our previous 12 Fr devices. Fig. 17(A) shows a 90°, 6-cm B-scan of the left atrium (LA) and a pulmonary vein (PV). Fig. 17(B) is a simultaneous, orthogonal B-scan showing the LA, right atrium (RA), aorta (A), and coronary arteries (CA).

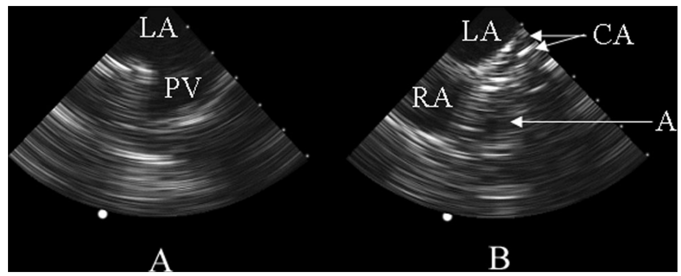

Fig. 17. 90°, 6 cm in vivo sheep heart images: (A) B-scan with imaging catheter in the coronary sinus showing left atrium (LA) and pulmonary vein (PV). (B) Simultaneous, orthogonal B-scan showing LA, right atrium (RA), aorta (A), and coronary arteries (CA).

IV. Conclusions

The design, fabrication and testing of two 7 Fr, 5 MHz, 112 channel, 2-D catheter arrays have been described, including 3-D images of tissue-mimicking phantoms as well as intracardiac images acquired during in vivo sheep studies. The catheter transducer has improved image quality and clinical utility in comparison to the previous designs due to its higher channel count, reduced size, and increased flexibility. These improvements were achieved by using a multisignal layer polyimide interconnect circuit and a noncoaxial, ribbon-based, high-density catheter cabling interconnection.

Limitations in the design and performance were mainly due to the small size of the 7 Fr catheter lumen. The small size of the acoustic aperture caused the acoustic beam to diverge at a constant angle beyond the far field transition distance of 2–4 mm, limiting the lateral resolution. One possible solution would be to increase the operating frequency of the transducer. We previously reported 2-D transducer arrays operating at frequencies of up to 10 MHz [34], but we have not pursued the development of high-frequency, intracardiac 2-D arrays due to system limitations at these higher frequencies.

We also have developed a matching layer for our 2-D catheter array, which improved the experimental element sensitivity by 3 dB, but our bandwidth was limited by the inability to inject any appreciable amount of acoustic backing in the 1.98-mm inner diameter of the catheter lumen. Further improvements in the acoustic performance of our 2-D arrays could be achieved by using multiple matching layers and thinner flex circuits so that more acoustic backing could be used.

Acknowledgments

The authors would like to thank W. L. Gore & Associates for providing the MicroFlat^{TM} catheter cabling, and MicroConnex for their assistance in developing the flexible interconnect circuit. The authors also thank Ned Light and Jesse Yen for their helpful input on transducer fabrication, and Ellen Dixon-Tulloch for her assistance during the in vivo studies. The authors would also like to thank Jason J. Hwang and Guidant Corporation for providing the 7 Fr catheter lumens.

References

[1] T. Bartel, S. Muller, G. Caspari, and R. Erbel, "Intracardiac and intraluminal echocardiography: Indications and standard approaches," *Ultrasound Med. Biol.*, vol. 28, pp. 997–1003, 2002.
[2] E. Chu, A. P. Fitzpatrick, M. C. Chin, K. Sudhir, P. G. Yock, and M. D. Lesh, "Radiofrequency catheter ablation guided by

intracardiac echocardiography," *Circulation*, vol. 89, pp. 1301–1305, 1994.

[3] J. F. Ren, F. E. Marchlinski, D. J. Callans, and H. C. Herrmann, "Clinical use of Acunav diagnostic ultrasound catheter imaging during left heart radiofrequency ablation and transcatheter closure procedures," *J. Amer. Soc. Echocardiogr.*, vol. 15, pp. 1301–1308, 2002.

[4] Z. M. Hijazi, Z. Wang, Q. L. Cao, P. Koenig, D. Waight, and R. Lang, "Transcatheter closure of atrial septal defects and patent foramen ovale under intracardiac echocardiographic guidance: Feasibility and comparison with transesophageal echocardiography," *Cathet. Cardiovasc. Intervent.*, vol. 52, pp. 194–199, 2001.

[5] C. J. Bruce, R. A. Nishimura, C. S. Rihal, D. J. Hagler, S. T. Higano, J. B. Seward, and D. R. Holmes, "Intracardiac echocardiography in the interventional catheterization laboratory: Preliminary experience with a novel, phased-array transducer," *Amer. J. Cardiol.*, vol. 89, pp. 635–640, 2002.

[6] J. M. Cooper and L. M. Epstein, "Use of intracardiac echocardiography to guide ablation of atrial fibrillation," *Circulation*, vol. 104, pp. 3010–3013, 2001.

[7] W. T. Abraham, W. G. Fisher, A. L. Smith, D. DeLurgio, A. Leon, E. Loh, D. Kocovic, A. Clavell, D. Hayes, A. Tang, V. Manda, and S. Petersen-Stejskal, "Long-term improvement in functional status, quality of life and exercise capacity with cardiac resynchronization therapy: The MIRACLE Trial experience," *J. Amer. Coll. Cardiol.*, vol. 39, no. 5A, p. 159A, 2002.

[8] W. T. Abraham, W. G. Fisher, A. L. Smith, D. DeLurgio, E. Loh, A. Leon, D. Kocovic, A. Clavell, and D. Hayes, "Cardiac resynchronization therapy reduces morbidity in patients with moderate to severe systolic heart failure and intraventricular conduction delays," *J. Amer. Coll. Cardiol.*, vol. 39, no. 5A, p. 171A, 2002.

[9] H. Izutani, K. J. Quan, L. A. Biblo, and I. S. Gill, "Biventricular pacing for congestive heart failure: Early experience in surgical epicardial versus coronary sinus lead placement," *Heart Surg. Forum*, vol. 6, pp. 1–6, 2003.

[10] C. J. Bruce, D. L. Packer, and J. B. Seward, "Intracardiac Doppler hemodynamics and flow: New vector phased array ultrasound tipped catheter," *Amer. J. Cardiol.*, vol. 83, pp. 1509–1512, 1999.

[11] C. J. Bruce, D. L. Packer, M. Belohlavek, and J. B. Seward, "Intracardiac echocardiography: Newest technology," *J. Amer. Soc. Echocardiogr.*, vol. 13, pp. 788–795, 2000.

[12] S. W. Smith, H. G. Pavy, and O. T. von Ramm, "High-speed ultrasound volumetric imaging system-part I: Transducer design and beam steering," *IEEE Trans. Ultrason., Ferroelect., Freq. Contr.*, vol. 38, pp. 100–108, 1991.

[13] O. T. von Ramm, S. W. Smith, and H. G. Pavy, "High-speed ultrasound volumetric imaging system—Part II: Parallel processing and image display," *IEEE Trans. Ultrason., Ferroelect., Freq. Contr.*, vol. 38, pp. 109–115, 1991.

[14] M. A. Schmidt, C. J. Ohazama, K. O. Agyeman, R. Z. Freidlin, M. Jones, J. M. Laurienzo, C. L. Brenneman, A. E. Arai, O. T. von Ramm, and J. A. Panza, "Real-time three dimensional echocardiography for measurement of left ventricular volumes," *Amer. J. Cardiol.*, vol. 84, pp. 1434–1439, 1999.

[15] G. Camarano, M. Jones, R. Z. Freidlin, and J. A. Panza, "Quantitative assessment of left ventricular perfusion defects using real-time three-dimensional myocardial contrast echocardiography," *J. Amer. Soc. Echocardiogr.*, vol. 15, pp. 206–213, 2002.

[16] M. Ahmad, T. R. Xie, M. McCulloch, G. Abreo, and M. Runge, "Real-time three dimensional dobutamine stress echocardiography in assessment of ischemia: Comparison with two-dimensional dobutamine stress echocardiography," *J. Amer. Coll. Cardiol.*, vol. 37, pp. 1303–1309, 2001.

[17] C. J. McCreery, M. McCulloch, M. Ahmad, and C. R. deFilippi, "Real-time 3-dimensional echocardiography imaging for right ventricular endomyocardial biopsy: A comparison with fluoroscopy," *J. Amer. Soc. Echocardiogr.*, vol. 14, pp. 927–933, 2001.

[18] H. Tsujino, M. Jones, T. Shiota, J. X. Qin, N. L. Greenberg, L. A. Cardon, A. J. Morehead, A. D. Zetts, A. Travaglini, F. Bauer, J. A. Panza, and J. D. Panza, "Real-time three-dimensional color Doppler echocardiography for characterizing the spatial velocity distribution and quantifying the peak flow rate in the left ventricular outflow tract," *Ultrasound Med. Biol.*, vol. 27, pp. 69–74, 2001.

[19] C. E. Fleishman, J. Li, T. Ota, C. J. Ohazama, G. Stetten, D. Adams, O. T. von Ramm, and J. Kisslo, "Identification of congenital heart defects using real time three-dimensional echo in pediatric patients," *Circulation*, vol. 94, 1996.

[20] E. D. Light, S. F. Idriss, P. D. Wolf, and S. W. Smith, "Real time three dimensional intracardiac echocardiography," *Ultrasound Med. Biol.*, vol. 27, pp. 1177–1183, 2001.

[21] G. D. Stetten, T. Ota, and C. J. Ohazama, "Real-time 3D ultrasound: A new look at the heart," *J. Cardio. Diag. Proc.*, vol. 15, pp. 73–84, 1998.

[22] E. D. Light, R. E. Davidsen, J. O. Fiering, T. A. Hruschka, and S. W. Smith, "Progress in two-dimensional arrays for real-time volumetric imaging," *Ultrason. Imag.*, vol. 20, pp. 235–250, 1998.

[23] J. O. Fiering, P. Hultman, W. Lee, E. D. Light, and S. W. Smith, "High-density flexible interconnect for two-dimensional ultrasound arrays," *IEEE Trans. Ultrason., Ferroelect., Freq. Contr.*, vol. 47, pp. 764–770, 2000.

[24] S. W. Smith, E. D. Light, S. F. Idriss, and P. D. Wolf, "Feasibility study of real-time three-dimensional intracardiac echocardiography for guidance on interventional electrophysiology," *PACE*, vol. 25, pp. 251–257, 2002.

[25] W. Lee and S. W. Smith, "Intracardiac catheter 2-D arrays on a silicon substrate," *IEEE Trans. Ultrason., Ferroelect., Freq. Contr.*, vol. 49, pp. 415–422, 2002.

[26] W. L. Lee and S. W. Smith, "Dual lumen transducer probes for real time 3D interventional cardiac ultrasound," *Ultrasound Med. Biol.*, vol. 29, pp. 1297–1304, 2003.

[27] J. A. Jensen and N. B. Svendsen, "Calculation of pressure fields from arbitrarily shaped, apodized, and excited ultrasound transducers," *IEEE Trans. Ultrason., Ferroelect., Freq. Contr.*, vol. 39, pp. 262–267, 1992.

[28] R. Krimholtz, D. A. Leedom, and G. L. Matthaei, "New equivalent circuits for elementary piezoelectric transducers," *Electron. Lett.*, vol. 6, pp. 398–399, 1970.

[29] J. Strole, S. Corbett, W. Lee, and S. Smith, "A novel flex circuit area-array interconnect system for a catheter-based ultrasound transducer," in *Proc. IMAPS Int. MicroElectronic Packaging Soc. Meeting*, 2002, pp. 453–458.

[30] R. E. Davidsen and S. W. Smith, "Two-dimensional arrays for medical ultrasound using multi-layer flexible circuit interconnection," *IEEE Trans. Ultrason., Ferroelect., Freq. Contr.*, vol. 45, pp. 338–348, 1998.

[31] M. G. Grewe, T. R. Gururaja, T. R. Shrout, and R. E. Newnham, "Acoustic properties of particle/polymer composites for ultrasonic transducer backing applications," *IEEE Trans. Ultrason., Ferroelect., Freq. Contr.*, vol. 37, pp. 506–514, 1990.

[32] C. Oakley, J. Mueller, D. Dietz, and J. Kuhnke, "A minimally invasive ultrasound probe using non-coax cabling," in *Proc. IEEE Ultrason. Symp.*, 2001, pp. 1011–1016.

[33] S. W. Smith and H. Lopez, "A contrast-detail analysis of diagnostic ultrasound imaging," *Med. Phys.*, vol. 8, pp. 4–12, 1982.

[34] E. D. Light, P. A. Hultman, S. F. Idriss, W. Lee, P. D. Wolf, and S. W. Smith, "Two dimensional arrays for real time volumetric and intracardiac imaging with simultaneous electrocardiagram," in *Proc. IEEE Ultrason. Symp.*, 2001, pp. 1195–1198.

Warren Lee was born in Orange County, CA, on September 27, 1976. He received a B.S.E. degree in biomedical and electrical engineering in 1998, and a Ph.D. degree in biomedical engineering in 2003, all from Duke University in Durham, NC.

He currently is working as an ultrasound engineer in the Ultrasound and Biomedical Laboratory at GE Global Research Center in Niskayuna, NY. His research interests include capacitive micromachined ultrasound transducers and the design of transducers for intracardiac echocardiography. Dr. Lee is a member of the IEEE.

Salim F. Idriss is an assistant professor of Pediatric Cardiology and Electrophysiology and an assistant professor of biomedical engineering at Duke University, Durham, NC. He obtained his undergraduate degree in biomedical engineering as well as his medical and graduate degrees at Duke University.

Dr. Idriss has over 10 years of experience and expertise in basic cardiac electrophysiology, arrhythmias, pacing, and defibrillation research. His research focuses on understanding arrhythmia vulnerability in infants, children, and adolescents. In addition, he also has research interest in developing new methods of catheter tracking and visualization for interventional electrophysiologic procedures. Dr. Idriss' clinical practice focuses on arrhythmia management and interventional electrophysiology in the young.

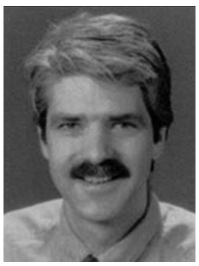

Patrick D. Wolf (M'89) was born in Altoona, PA, in 1956. He received a B.S. degree in electrical engineering and an M.S. degree in bioengineering from the Pennsylvania State University, State College, PA. After receiving his Ph.D. degree from Duke University, Durham, NC, in 1992, he joined the faculty in biomedical engineering and is currently pursuing his research interests in instrumentation, cardiac arrhythmias, and the brain-machine interface.

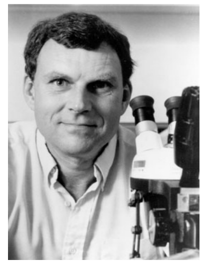

Stephen W. Smith (M'91) was born in Covington, KY, on July 27, 1947. He received the B.A. degree in physics (summa cum laude) in 1967 from Thomas More College, Ft. Mitchell, KY, the M.S. degree in physics in 1969 from Iowa State University, Ames, and the Ph.D. degree in biomedical engineering in 1975 from Duke University, Durham, NC.

In 1969, he became a Commissioned Officer in the U.S. Public Health Service, assigned to the Food and Drug Administration, Center for Devices and Radiological Health, Rockville, MD, where he worked until 1990 in the study of medical imaging, particularly diagnostic ultrasound and in the development of performance standards for such equipment. In 1978, he became an adjunct associate professor of radiology at Duke University Medical Center. In 1990, he became an associate professor of biomedical engineering and radiology, and Director of Undergraduate Studies in Biomedical Engineering at Duke University. He holds 16 patents in medical ultrasound and has authored 100+ publications in the field.

Dr. Smith is cofounder of Volumetrics Medical Imaging. He has served on the education committee of the American Institute of Ultrasound in Medicine, the executive board of the American Registry of Diagnostic Medical Sonographers, the editorial board of *Ultrasonic Imaging*, and the Technical Program Committee of IEEE-UFFC. He was corecipient of the American Institute of Ultrasound in Medicine Matzuk Award in 1988 and 1990 and corecipient of the IEEE-UFFC Outstanding Paper Award in 1983 and 1994.